Int. J. Microgravity Sci. Appl., **33** (2) (2016) 330215
DOI: 10.15011/jasma.33.330215

IIIII ISPS-6 Proceedings IIIII
(Original Paper)

Containerless Processing of Metastable Multiferroic Composite in R-Fe-O System (R: Rare-earth element)

Kazuhiko KURIBAYASHI [1,2], Ryota TAKAHASHI [1], Yuko INATOMI [2], Shumpei OZAWA [1] and M. S. VIJAYA KUMAR [2,3]

Abstract

The hexagonal structure with a space group of $P6_3cm$ has been known to be stable in the $RMnO_3$ system (R: rare earth element) of the rare earth elements having smaller ionic radius. The hexagonal $RMnO_3$ (h-$RMnO_3$) has attracted great interest towards their wide applications in the field of electronic industry, because h-$RMnO_3$ shows multiferroic properties such as ferroelectricity, ferromagnetism and ferroelasticity in the same phase. Nevertheless, the materials for practical applications remain undeveloped, because h-$RMnO_3$ shows anti-ferromagnetism as well as low magnetic transformation temperature below 100 K. To solve this problem, we considered that a composite of a ferromagnetic phase and a ferroelectric phase is more realistic than a single-phase material. On the basis of this idea, we attempted to synthesize the multiferroic composite consisting of ferroelectric h-$RFeO_3$ and ferromagnetic Fe_3O_4 by utilizing the containerless technique. The experimental result showed that it is possible to exhibit a fine composite structure when h-$LuFeO_3$ and Fe_3O_4 are equimolar amounts. However, the orthorhombic phase (o-$RFeO_3$) as well as h-$RFeO_3$ was observed in the samples in which the mole-fraction of Fe_3O_4 was increased. The reason for forming the o-$RFeO_3$ phase is attributed to the decrease of the driving force for forming a metastable phase due to the fact that the solute atom or molecule is redistributed at the solid-liquid interface of the growing crystal.

Keyword(s): Containerless processing, Undercooling, Rapid solidification, Multiferroic materials
Received 20 September 2015, Accepted 30 December 2015, Published 30 April 2016

1. Introduction

Multiferroicity is a general term for a phenomenon that multiple "ferroic" properties such as ferromagnetic, ferroelastic and ferroelectric properties are included in one system and there is a strong correlation between these properties. Many studies[1)] on materials that are ferromagnetic and ferroelectric have been reported since these materials can be expected as a storage medium. That is, the electric field controls the spin-arrangement and the magnetic field controls the electric polarization, in the same device. In particular, hexagonal rare-earth manganite with a space group of $P6_3cm$ (h-$RMnO_3$, R: Dy-Lu and Y) has been attracting attention as a promising candidate for this objective in recent years[2)]. However, h-$RMnO_3$ is unsuited for practical use because the magnetic transition temperature is as low as 100 K and the magnetic properties are antiferromagnetic. In order to make practical multiferroic materials, it is essential to search for materials exhibiting ferromagneticity and ferroelectricity simultaneously.

Previously we carried out the experiment of containerless processing under controlled oxygen partial pressure using rare-earth transition metal sesqui oxide as the sample and reported that the same hexagonal phase as h-$RMnO_3$ is formed as a metastable h-$RFeO_3$ phase in $YbFeO_3$ and $LuFeO_3$[3,4)]. We also reported that in as-solidified samples, fine eutectic lamellar-structure with a magnetic phase of Fe_3O_4 exists at the grain boundary despite that the solidified structure is macroscopically single-phase of h-$RFeO_3$. This microstructure, although it goes against the original definition of multiferroicity that simultaneously possesses both ferromagnetic and ferroelectric natures within one phase, inspired us as a candidate for the multiferroic nano-composite in terms of forming a lamellar structure of both phases. From this point, by considering the chemical composition, that is, the ratio of Fe^{3+} and R^{3+}, we aimed to examine the possibility of the nano-composite.

2. Experimental procedure

Since h-$RFeO_3$ is a metastable phase, it is required that the melt is cooled below the equilibrium melting temperature and solidified from this state. **Figure 1** shows the schematic diagram of an experimental apparatus, an aerodynamic levitation furnace (ADL), which was used in this study. Since the objective of the present investigation is to fabricate the fine composite of Fe_3O_4

1 Department of Advanced Materials Science and Engineering, Chiba Institute of Technology, Tsudanuma, Narashino, Chiba275-0016, Japan.
2 Institute of Space and Astronautical Science, JAXA, Yoshinodai, Chuo-ku, Sagamihara, Kanagawa252-5210, Japan.
3 Department of Mechanical Engineering, Tufts University, Medford, MA02155, USA.
(E-mail: Corresponding author: k_kuribayashi@nifty.com)

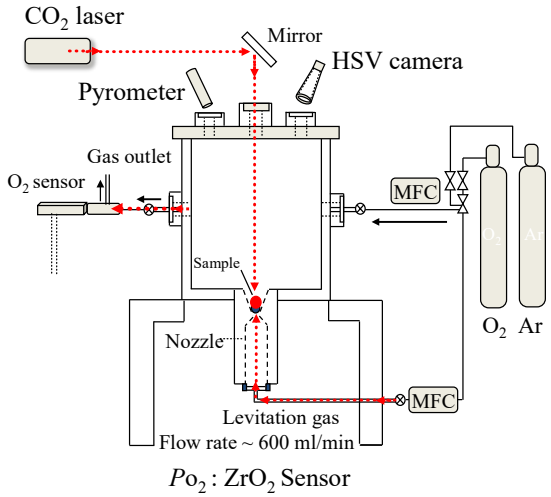

Fig. 1 Schematic diagram of an aerodynamic levitation furnace (ADL). The angle and the orifice of the conical nozzle are 60° and 1mmϕ, respectively.

and *h*-$RFeO_3$ as described above, Lutetium was selected in this study as a rare earth element in $RFeO_3$ based on the experimental results of our previous paper[5]. Three kinds of samples, $LuFe_2O_{4+x}$, $LuFe_3O_{5+y}$ and $LuFe_4O_z$ (z~7), which are different in the ratio between Lu and Fe ions, were prepared. In addition, $LaFe_2O_{4+x}$ and YFe_2O_{4+x} samples where the ionic radii of rare-earth elements are larger than that of $LuFe_2O_{4+x}$ were also prepared in order to examine the influence of ionic radius of rare-earth element on the phase selection.

Controls of oxygen partial pressure Po_2 and the heating temperature are indispensable in forming the composite of $LuFeO_3$ and Fe_3O_4. Katsura *et al.*[6] reported the following chemical reactions the phase equilibrium of $LuFeO_3$ and Fe_3O_4:

$$6LuFe_2O_4 + O_2 = 6LuFeO_3 + 2Fe_3O_4$$
$$\Delta G = -203760 \text{ J/mol} \qquad T = 1523 \text{ K} \qquad (1)$$

$$18LuFeO_3 + 4Fe_3O_4 + O_2 = 6Lu_3Fe_5O_{12}$$
$$\Delta G = -89496 \text{ J/mol} \qquad T = 1473 \text{ K} \qquad (2)$$

$$6Lu_2Fe_3O_7 + O_2 = 12LuFeO_3 + 2Fe_3O_4$$
$$\Delta G = -196194 \text{ J/mol} \qquad T = 1523 \text{ K} \qquad (3)$$

where ΔG is the free energy change of the reaction. If ΔG is approximated by a linear function of temperature T as $A+BT$, A and B correspond to the enthalpy change ΔH and the entropy change ΔS, respectively. In the above equations, if it is assumed that ΔS is equal to the decrease of entropy caused by vanishing of 1 mole of oxygen gas (that is equal to -205.1 J/mol·K), ΔH of Eqs. 1, 2 and 3 are given by -516.1 kJ/mol, -391.6 kJ/mol and -508.6 kJ/mol, respectively.

In addition, the stability of Fe_3O_4 is described by the following chemical reactions[7]:

$$3FeO + 1/2\ O_2 = Fe_3O_4$$
$$\Delta G = -312200 + 125.0\ T \text{ (J/mol)} \qquad (4)$$

$$2Fe_3O_4 + 1/2\ O_2 = 3Fe_2O_3$$
$$\Delta G = -249500 + 140.7\ T \text{ (J/mol)} \qquad (5)$$

These reactions were obtained in a solid state. However, if these reactions can be extended to the liquid state, the temperatures at which Eqs. 1, 2 and 3 are equilibrated are 2516 K, 1919 K and 2480 K, respectively. In the same way, the temperatures are respectively derived to be 1773 K and 2498 K from Eqs. 4 and 5. On the basis of these results, heating temperature was determined as 2273 K. Although the processing was mainly carried out at Po_2 of 10^5 Pa, 10^3 Pa and 10^{-1} Pa were partly employed in order to examine the influence of Po_2 on the phase selection.

High purity (99.99%) powders of R_2O_3 and Fe_2O_3 were used as raw materials. These powders were weighed so that the molar fraction of each powder in mixed state may be the predetermined values. Then, we melted the powder using a semiconductor laser and formed a spherical sample of 2 mm in diameter. After putting the sample into the conical nozzle that was fixed in the chamber of ADL, we evacuated the chamber up to 1.0×10^{-1} Pa. Then, after the chamber was filled to 10^5 Pa by mixed gas of high purity O_2 and Ar, which were adjusted to be the predetermined values of Po_2, the sample was levitated by controlling the flow rate of the mixed gas and was melted by CO_2 laser. After being heated up to 2273 K, and held for approximately 30 seconds, the sample was cooled by turning off the laser beam and solidified.

The temperature of the sample was measured by a dual-color pyrometer with a sampling rate of 100 Hz and the solidification sequences were observed at 1000 frames per second with a high-speed video camera (HSV). The surface morphologies, crystal structures, cross-sectional microstructures and magnetic transition temperatures of solidified samples were examined by laser scanning microscope (LSM), scanning electron microscope (SEM), X-ray diffractometry (XRD) of Cu$K\alpha$ and vibrating sample magnetometer (VSM), respectively.

3. Results

3.1 Observation of solidification behavior by HSV

Figure 2 shows the images taken by using HSV during recalescence that occurred in the sample of RFe_2O_{4+x} at Po_2 of 10^5 Pa. In these images, bright area and dark area correspond to the solid phase and liquid phase, respectively. The numerals shown at the top of each image are the elapsed time in seconds from the beginning of recalescence. In our previous work[8], we

reported that the growth rate of $RFeO_3$ decreases in the order of La, Y and Lu along the periodic table. However, the growth rate in the sample of RFe_2O_{4+x} has changed irregularly: That is, although the growth rates of $LaFe_2O_{4+x}$ and $LuFe_2O_{4+x}$ were nearly equal, the growth rate of YFe_2O_{4+x} was approximately half of others. In this way, no systematic differences were observed in the growth rates: The reason for this behavior may be attributed to the long-range diffusion induced by the partitioning of constituents at the solid-liquid interface of the growing crystal.

The interface of $LaFe_2O_{4+x}$ showed a smooth curve. However, the interface in YFe_2O_{4+x} changed to a wavy shape of small amplitude. On the other hand, the interface in $LuFe_2O_{4+x}$ changed irregular and looked polyhedral. This polyhedral surface was also observed in $LuFe_3O_{5+y}$ and $LuFe_4O_z$.

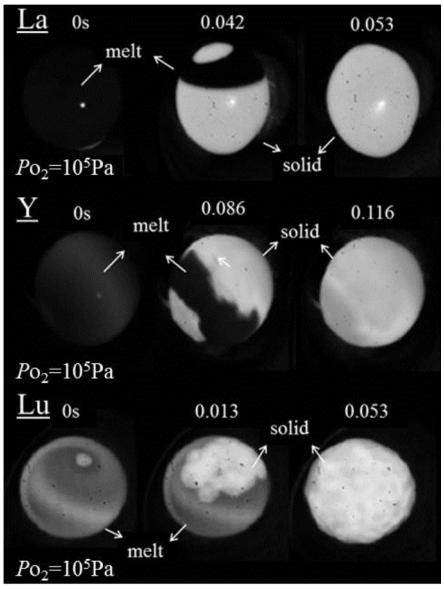

Fig. 2 Typical recalescence behaviors in RFe_2O_{4+x} (R: La, Y and Lu) were observed by using HSV. All the samples solidified spontaneously at Po_2 of 1×10^5 Pa. The frames are taken at time intervals of 0.001 s and elapsed time is indicated at the top of each photograph.

3.2 Temperature measurement by pyrometer

Figure 3 shows the relation between temperature and time at the recalescence stage corresponding to the HSV images shown in **Fig. 2**. If the temperature at which the recalescence starts is assumed to be the nucleation temperature, the degree of undercooling became smaller in the order of $LaFe_2O_{4+x}$ and YFe_2O_{4+x} and became smallest in $LuFe_2O_{4+x}$ in the same way as in $RFeO_3$ where the hexagonal phase was formed[8].

Figure 4 shows the temperature-time relations of $LuFe_2O_{4+x}$, $LuFe_3O_{5+y}$ and $LuFe_4O_z$ samples at Po_2 of 10^5 Pa, respectively. If the temperature after recalescence is assumed to be the melting temperature or the liquidus temperature of the material, increasing the concentration of Fe ions induces the decrease of the melting point, suggesting that the phase diagram of $LuFeO_3$-Fe_3O_4 is eutectic.

3.3 Surface observation byLSM

Figure 5 shows the micrographs of the samples taken by LSM. These samples were processed at Po_2 of 10^5 Pa. The surface morphology, although depending on Po_2 are approximately classified into three Types, Type I, Type II and Type III, respectively: Type I is constituted with a rough surface like a summer orange; Type II is macroscopically a

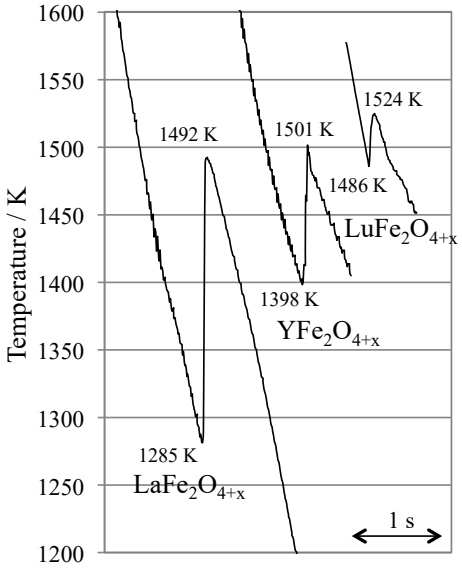

Fig. 3 Typical cooling curves of RFe_2Osamples (R: La, Y and Lu) solidified spontaneously at Po_2 of 1×10^5 Pa.

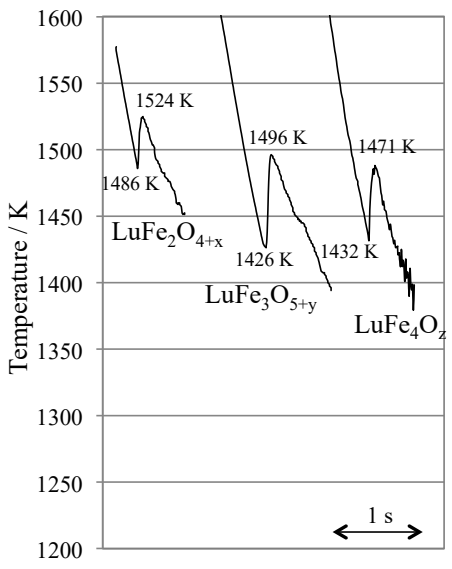

Fig. 4 Typical cooling curves$LuFe_2O$, $LuFe_3O$ and samples solidified spontaneously at Po_2 of 1×10^5 Pa.

polyhedral shape, but microscopically a dendritic shape; and Type III is a typical polyhedron constituted by faceted planes. The surfaces of $LaFe_2O_{4+x}$ a nd $LuFe_2O_{4+x}$ belong to Type I and Type III, respectively. On the other hand, YFe_2O_{4+x} was Type II that suggests the occurrence of double recalescence as in $YFeO_3$[5]. These features are well consistent with the HSV images.

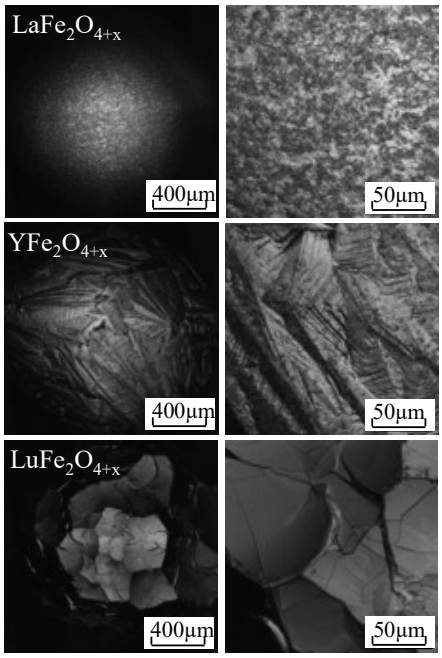

Fig. 5 Laser scanning micrographs of the surface of the RFe_2Osamples (R: La, Y and Lu) solidified spontaneously at 1×10^5 Pa of P_{O2}.

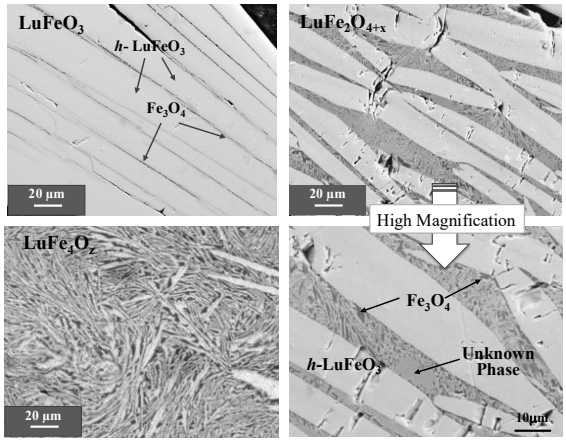

Fig. 6 Cross-sectional microstructures of as-solidified samples of $LuFeO_3$, $LuFe_2O$ and $LuFe_4O_z$. Each sample was solidified at P_{O2} of 1×10^5 Pa. The figure at the lower right is the magnified image of the figure at the upper right. It is clear that the proportion of the grain boundary phase in $LuFe_2O_{4+x}$ is larger than that in $LuFeO_3$: This result shows that the increase of Fe concentration increases the volume fraction of the grain boundary phase. However, the photograph with high magnification shows that there exists the unknown phase in grain boundary region.

3.4 Microstructure observation by SEM

Figure 6 shows the cross-sectional microstructures of $LuFe_2O_{4+x}$ and $LuFe_4O_z$ samples that solidified at P_{O2} of 10^5 Pa. The photograph of $LuFeO_3$ is also shown as an example of the *h*-$RFeO_3$ phase. As shown in this image, the volume fraction of the grain boundary phase in $LuFe_2O_{4+x}$ samples is larger than that in $LuFeO_3$ samples. However, *h*-$RFeO_3$ was still the primary phase and remained as a coarsened grain. Furthermore, as can be seen from the photograph of high magnification, the grain-boundary phase was not a eutectic phase between *h*-$RFeO_3$ and Fe_3O_4 but a eutectic phase between Fe_3O_4 and an unknown phase. On the other hand, the grain size remarkably diminished in $LuFe_4O_z$, although the primary phase and the grain boundary phase were respectively $RFeO_3$ and the eutectic phase between the unknown phase and Fe_3O_4 as in $LuFe_2O_{4+x}$. From the difference in the blackness of the microstructure, we can estimate the density of Fe ion in respective microstructures: that is, the density of Fe ion in this unknown phase is larger than that in *h*-$RFeO_3$ but smaller than that in Fe_3O_4.

3.5 XRD analysis

Figure 7 shows the XRD patterns of as-solidified RFe_2O_{4+x} samples. The decisive features of the standard XRD pattern of

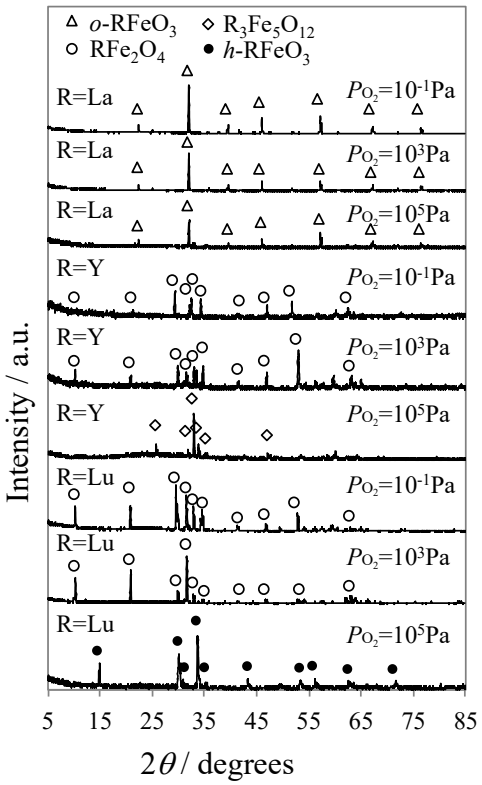

Fig. 7 X-ray diffraction patterns of the as-solidified RFe_2O samples (R: La, Y and Lu) processed at various P_{O2} of 1×10^{-1} Pa, 1×10^3 Pa and 1×10^5 Pa. The characteristic difference in XRD pattern of *h*-$RFeO_3$ and *o*-$RFeO_3$ whether the s exist at approximately 43° and 15° in 2θ According to this criterion, *h*-$RFeO_3$ appears only in $LuFe_2O$ samples solidified at P_{O2} of 1×10^5 Pa.

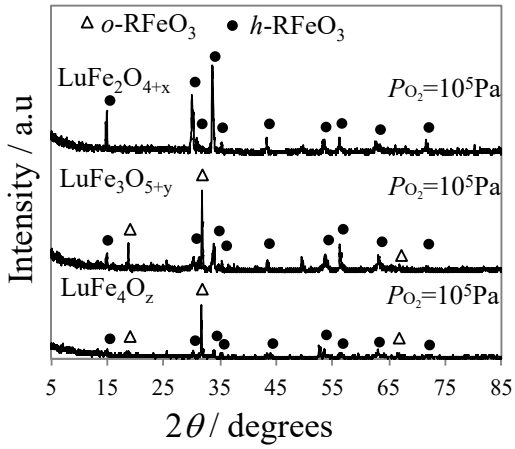

Fig. 8 X-ray diffraction patterns of the as-solidified samples of $LuFe_2O$, $LuFe_3O$ and $LuFe_4O$. In LuFe3O5+y and LuFe4Oz, not only *h*-$RFeO_3$ but also *o*-$RFeO_3$ appears. Furthermore, in $LuFe_4O$, *h*-$RFeO_3$ seems to be diminished slightly and *o*-$RFeO_3$ becomes predominant.

h-$RMnO_3$ are the existence of the two peaks of high intensity that appear at approximately 15° and 43° in 2θ. These peaks never appear in *o*-$RMnO_3$. In this regard, *h*-$RFeO_3$ was formed only in the $LuFe_2O_{4+x}$ sample that was solidified at P_{O2} of 10^5 Pa: that is, $LaFe_2O_{4+x}$ showed a pattern of *o*-$RFeO_3$ irrespective of P_{O2}. In YFe_2O_{4+x}, YFe_2O_4 was shown in the samples formed at 10^3 Pa and 10^{-1} Pa of P_{O2}. Furthermore, the garnet phase ($Y_3Fe_5O_{12}$) was identified in the sample formed at P_{O2} of 10^5 Pa. **Figure 8** shows the XRD patterns for $LuFe_2O_{4+x}$, $LuFe_3O_{5+y}$ and $LuFe_4O_z$ processed at P_{O2} of 10^5 Pa. As shown in this figure, although *h*-$RFeO_3$ can be observed in all the three $LuFe_2O_{4+x}$, $LuFe_3O_{5+y}$ $LuFe_4O_z$ samples, *o*-$RFeO_3$ phase can be observed in both $LuFe_3O_{5+y}$ and $LuFe_4O_z$ sample. Although the XRD peak of Fe_3O_4 was unidentified because of the luminescence from Fe ion excited by Cu*K*α, the unknown phase is inferred to be *o*-$RFeO_3$.

3.6 Thermo-magnetic analysis

In order to confirm the unknown phase that was suggested by SEM and XRD analysis, the temperature dependence of the magnetization of the sample was measured. **Figure 9** shows the relation between magnetization and temperature at the heating and cooling stages of the as-solidified sample of $LuFe_2O_{4+x}$. The datum of $LuFeO_3$ was also shown for comparison. In this analysis, magnetization was measured under the magnetic field of 0.05T.

Although the significant magnetic transition that supports the existence of the Fe_3O_4 phase was observed at 848 K in the heating stage of the as-solidified sample of $LuFeO_3$, at the cooling stage the Fe_3O_4 phase was already annealed out and the sample had become almost the single phase of *h*-$RFeO_3$. On the other hand, not only the magnetic transition of Fe_3O_4 but also the magnetic transition at 623 K that indicates the existence of the *o*-$LuFeO_3$ was observed in the sample of $LuFe_2O_{4+x}$. Namely, increasing the amount of Fe ions stabilizes *o*-$LuFeO_3$ as well as Fe_3O_4.

4. Discussion

As mentioned in the introduction, the present investigation aims at establishing the chemical composition that is best suited for forming nano-scaled composites of Fe_3O_4 and *h*-$RFeO_3$. The experimental result showed that increasing the ratio between Fe to Lu induces the increase of the volume fraction of the fine eutectic structure between Fe_3O_4 and *h*-$RFeO_3$. However, the increase in volume fraction of Fe_3O_4 led to the precipitation of *o*-$RFeO_3$ in the grain boundary region. This result suggests that increasing Fe ion facilitates the *o*-$RFeO_3$ phase to nucleate even though the *h*-$RFeO_3$ phase can be nucleated as the primary phase. This situation looks similar with the double recalescence observed in $YbFeO_3$[4].

We have reported the experimental verification of the criterion for forming the metastable phase from the undercooled

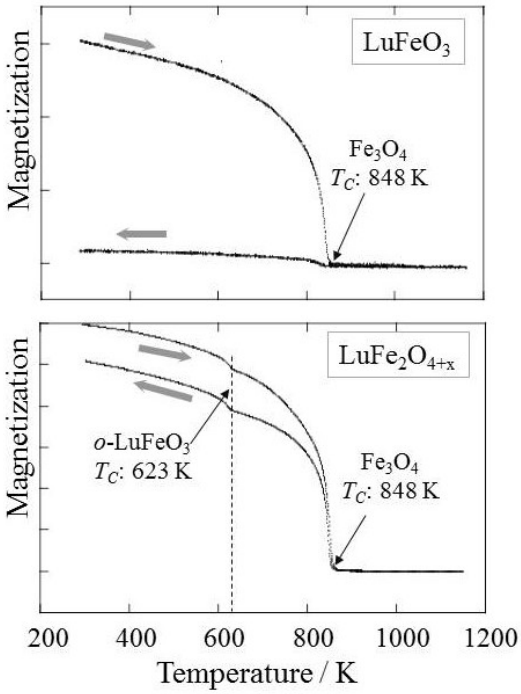

Fig. 9 Thermo-magnetization curves of samples of $LuFeO_3$ and $LuFe_2O_{4+x}$ solidified at P_{O2} of 1×10^5 Pa. Although a significant magnetic transition which indicates the existence of Fe_3O_4 was observed at 848 K in $LuFeO_3$, it has disappeared at the cooling stage. On the other hand, in $LuFe_2O_{4+x}$, magnetic transition which suggests the existence of *o*-$LuFeO_3$ was observed at 623 K. In addition, this transition survives even at the cooling stage, implying that the *o*-$LuFeO_3$ was stabilized by increasing the content of Fe ions.

melt in our recent paper[9]. In this paper, we also elucidated the reason for double recalescence as the competitive relation between two-dimensional nucleation of metastable phase and the three-dimensional heterogeneous nucleation of the stable phase. That is, if the energy barrier for subsequent growth of the metastable phase is larger than that for the heterogeneous nucleation of the stable phase, the stable phase will nucleate, showing double recalescence. In the single-phase material where the chemical composition of the solid phase is the same as that of the liquid phase, double recalescence occurs if the difference in melting temperatures between the stable phase and the metastable phase is large and the undercooling is smaller than the critical ones. However, in the multi-phase material, solute atom or molecule will be redistributed so as to satisfy the local equilibrium at the solid-liquid interface of growing crystal. As a result, the driving force for forming the metastable phase is reduced.

Figure 10 shows this situation. That is, in the AB binary molecular system showing the eutectic phase diagram, the chemical potential of component A decreases when the concentration of component B increases at the solid-liquid interface. If the increment of B is expressed as ΔC, the decrement of the chemical potential of A, $\Delta G^{s\text{-}ms}$, is given by

$$\begin{aligned}\Delta G^{s-ms} &= RT\left\{\left(1-C_{\mathrm{B}}-\Delta C\right)-\ln\left(1-C_{\mathrm{B}}\right)\right\} \\ &= RT\left(1-\frac{\Delta C}{1-C_{\mathrm{B}}}\right)\end{aligned} \quad . \qquad (6)$$

under the assumption of the ideal solution. If $\Delta C/(1-C_{\mathrm{B}})<<1$ is assumed, Eq. 6 is approximated by

$$\Delta G^{s-ms} \approx RT\frac{\Delta C}{1-C_{\mathrm{B}}}. \qquad (7)$$

Namely, Eq. 7 expresses the decrement of the driving force for forming the metastable phase. Although the driving force for forming the stable phase decreases similarly to that for the metastable phase, the ratio of the decrements to the driving forces is larger in the case of the metastable phase than in the case of the stable phase. As a result, even though *h*-$RFeO_3$ phase was initially formed from the undercooled melt, the *o*-$RFeO_3$ phase gradually becomes predominant.

In order to suppress the forming of the *o*-$RFeO_3$ phase, it is required to stabilize the *h*-$RFeO_3$ phase by varying the chemical composition; for instance, from Fe ion to Mn ion.

5. Conclusions

Hexagonal *h*-$RMnO_3$ with a space group of $P6_3cm$ has attracted a great interest in the field of electronic industry, due to the multiferroic characteristics that have both ferromagnetic and ferroelectric properties in one phase, which possess a latent potential towards a wide range of applications. However, materials for practical use have not been developed, since the magnetic property of *h*-$RMnO_3$ is antiferromagnetic. In this respect, we hypothesized that the nano-scaled composite with ferroelectric phase and the ferromagnetic phase is more realistic than getting a single-phase multiferroic property. Then, using Fe^{3+} of larger magnetic moment than Mn^{3+}, we attempted to synthesize the multiferroic composite by means of the containerless processing technique. As the base material, we used $LuFeO_3$ because we had published a paper concerning the formation of metastable *h*-$RFeO_3$. Taking account of the ratio of Lu to Fe and the oxygen partial pressure, we obtained the finely dispersed microstructure between *h*-$RFeO_3$ and Fe_3O_4. However, the increase in volume fraction of Fe_3O_4 led to the precipitation of *o*-$RFeO_3$ in the grain boundary region. Considering the influence of the chemical composition on the driving force for crystal nucleation, we have concluded that the reason for *o*-$RFeO_3$ to be formed can be ascribed to the decrease of the driving force for forming a metastable phase induced by the increase of the chemical composition at the solid-liquid interface of the growing crystal.

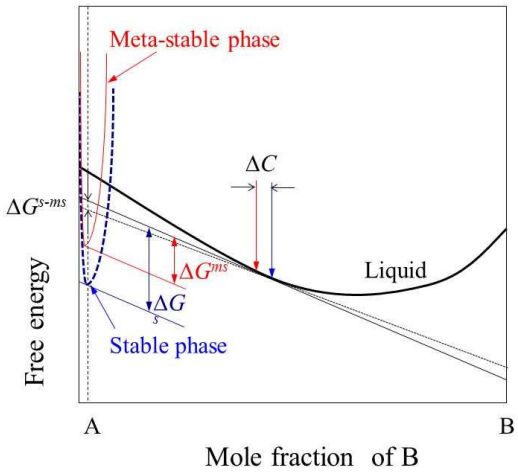

Fig. 10 Schematic presentation of eutectic phase diagram and the relation between free energy and the chemical composition. When the chemical composition of component B at the solid-liquid interface increases, the chemical potential of component A decreases. Growing of metastable phase reduces the driving force for continuing the growth of the metastable phase itself. The decrement of the driving force $\Delta G^{s\text{-}ms}$ is approximated by $RT\Delta C/(1\text{-}C_{\mathrm{B}})$.

Acknowledgments

This work was carried out under the financially support of Grant-in-Aid for Scientific Research from the Japan Society for the Promotion of Science. The authors express their sincere thanks here.

References

1) R. Ramesh and N. A. Spaldin : Nature Materials, **21** (2007) 6.
2) B. B. Van Aken, T. T. M. Palstra, A. Flippest and N. A. Spaldin: Nature Materials, **164** (2004) 3.
3) M.S. Vijaya Kumar, K. Kuribayashi and K. Kitazono: J. of Materials Research, **2996** (2008) 23.
4) M.S. Vijaya Kumar, K. Kuribayashi and K. Kitazono: J. of the American Ceramic Society, **903** (2009) 92.
5) K. Nagashio and K. Kuribayashi: J. of the American Ceramic Society, **2550** (2002) 85.
6) T. Katsura, T. Sekine, K. Kitayama, T. Sugihara and N. Kimizuka: J. Solid State Chemistry, **43** (1978) 23.
7) O. Kubaschewski and C.B. Alock: Metallurgical Thermochemistry, 5th Ed., Pergamon Press, **268** (1978).
8) M.S. Vijaya Kumar, K. Kuribayashi, T. Hibiya and S. Yoda: J. of the American Ceramic Society, **995** (2013) 96.
9) K. Kuribayashi, H. Kato, K. Nagayama, Y. Inatomi and M.S. Vijaya Kumar: J. of Applied Physics, **117** (2015) 154905.